2024-03-15

Experimental investigation of transient strains of GGBS-FA-SF blended geopolymer concrete at elevated temperatures

Yu, M

10.1016/j.conbuildmat.2024.135589
Construction and Building Materials
Elsevier

Experimental investigation of transient strains of GGBS-FA-SF blended geopolymer concrete at elevated temperatures

Min Yu[a,b], Tan Wang[b], Hanjie Lin[b], Dawang Li[c], Long-yuan Li[a,*]

a) School of Engineering, Computing and Mathematics, University of Plymouth, Plymouth PL4 8AA, UK
b) School of Civil Engineering, Wuhan University, Wuhan 430072, China
c) Guangdong Provincial Key Laboratory of Durability for Marine Civil Engineering, Shenzhen University, Shenzhen 518060, China
* Corresponding author

Abstract - Fire is one of the most severe conditions encountered during the lifetime of a structure. Consequently, the provision of proper fire safety measures for structural members is a major safety requirement in building design. In this paper an experimental study is reported on the axial deformation of GGBS-FA-SF blended geopolymer mortar and geopolymer concrete with and without steel fibre when they are subjected to both mechanical and thermal loadings. The transient tests were conducted in Instron machine with additional heating facility. During the test the specimen was first subjected to a pre-defined mechanical load and followed by thermal heating. The transient axial deformations of the tested specimens were recorded using digital image correlation camera. By using the experimentally obtained temperature-dependent thermal strains of the specimen with different preloads the transient strains of the geopolymer mortar and geopolymer concrete with and without steel fibre are analysed and evaluated. Finally, empirical formulas are also proposed to reproduce the influence of the preload, heating temperature and constituents of the mix on the transient strain of geopolymer mortar and geopolymer concrete.

Keywords: Geopolymer; Alkali activated binder; Concrete; Fire; Elevated temperature; Transient strain.

1 Introduction

Fire resistance of concrete structural members is conventionally determined through standard fire tests. In recent years, however, the prediction of using numerical methods becomes favourable because it is less time consuming and inexpensive. The key in evaluating the fire performance of a concrete structural member when using numerical methods is the temperature-dependent stress-strain relation of concrete materials [1]. Unlike the steel, concrete is a composite material composed mainly of water, aggregate and cement paste. Under the effect of fire, heat is transferred from fire exposed surface to the interior of concrete. The rise of temperature in concrete leads to a series of physical and chemical reactions of materials, which include thermal expansion, local stresses developed due to mismatched thermal expansions between aggregate and cement paste, pore pressure built-up due to evaporation of free water in capillary pores, expulsion of physically and chemically bound water, and dehydration and decomposition of cement hydration products. These reactions affect not only the mechanical properties but also lead the change of microstructures of concrete. Thus, the mechanical properties of a heated concrete depend on not only the fire temperature but also the level of preload and the composition and characteristics of the concrete material.

Research on the thermal expansion of ordinary Portland cement (OPC) concrete with and without preloading is vast [2,3] and dates back to 1960s when Hansen and Eriksson [4] found from their tests that the cement paste and mortar beams deflected excessively when heated after the application of a load. The most notable work perhaps is the experimental work carried out by Anderberg and Thelandersson in 1976 [5] that illustrated the effect of preload on the response of concrete cylinders. Since the mid of 1970s, great efforts have been made in identifying the deforming mechanisms occurred in concrete when different thermal and mechanical loading paths are applied, e.g., a mechanical load is applied first and followed by thermal heating (transient test) instead of the conventional loading path in which thermal heating is applied first and followed by mechanical loading (steady-state test). For example, Khoury [6,7,8] investigated the strain behaviour of OPC concrete during heating and cooling cycles for temperatures up to 600°C with and without applied load. Li and Purkiss [9] presented a review on the analysis models of stress-strain constitutive relationships of OPC concrete at elevated temperatures when the transient strain is considered. Youssef and Moftah [10] presented a stress-strain constitutive equation for concrete at high temperatures, which includes the compressive and tensile strengths, peak strain, elastic modulus, thermal and transient creep strains. Sadaoui and Khennane [11] reported a numerical study on the effect of transient creep on the behaviour of unrestrained reinforced concrete column using finite element method. Schneider and Schneider [12,13] proposed a transient concrete model for determining the restraint in concrete structures in fire, and carried out the experimental investigation on the model for concrete in compression at elevated temperatures. Toyoda et al. [14] experimentally examined the effect of high temperature on the mechanical properties of 100 MPa high-strength concrete. It was found that the effect of transient strain is bigger in the high-strength concrete than in the moderate strength concrete. Knaack et al. [15] reported a study on the compressive stress-strain behaviour of unreinforced concrete under high temperatures. Gernay and Franssen [16] proposed the formulation of the Eurocode 2 concrete material model, which includes an explicit term for transient creep. Huang and Burgess [17] presented an elevated temperature analysis on a Shanley-like column model to demonstrate the importance of considering transient strain in the analysis. Tao et al. [18] presented an experimental study on the self-compacting concrete specimens subjected to high temperatures when they are also mechanically loaded. Aslani [19] presented the formulations for estimating the parameters affecting the behaviour of unconfined and prestressed concrete at high temperatures. Nguyen and Tan [20] conducted the analytical and numerical analyses of eccentrically loaded columns restrained from thermal elongation in concrete framed structures in fire. Ožbolt et al. [21] presented a numerical analysis of reinforced concrete beams subjected to elevated temperatures followed by mechanical loading. The model was implemented into a 3-D finite element analysis code. Lu et al. [22] carried out a comparison analysis between the fire performances of simple supported members with implicit and explicit models. Hwang et al. [23] reported a numerical evaluation of the fire resistance of reinforced concrete structures. The analysis considered the temperature-dependent nonlinear material properties such as thermal, transient and creep strains, which increase with elevated temperature in fire. Lee et al. [24] experimentally examined the thermal strain behaviour and strength degradation of ultra-high strength concrete when exposed to elevated temperatures under loading conditions. Yoon et al. [25] evaluated the compressive strength, elastic modulus, and creep behaviour of preloaded high-strength concretes at various target temperatures. Yao et al. [26] presented a multiaxial plastic-damage constitutive model for concrete at different temperatures. The model was implemented in 3-D finite element analysis under fire conditions. Mahmoud [27] proposed different approaches to define concrete ultimate limit strain envelops at high temperatures for preloaded and unloaded, confined and unconfined columns during heating. Al-Thairy [28] presented an analytical method for thermal steady-state and transient analyses of hybrid steel and FRP-

reinforced concrete beams exposed to high temperatures. Zawadowska et al. [29] investigated the mechanical properties of concrete exposed to elevated temperatures by using both transient and non-transient tests. The experimental results were presented in terms of stress-strain relationships and critical temperatures. Fan et al. [30] reported the experimental results of steady-state and transient tests of OPC concretes with and without fly ash. Abubaker and Davie [31] presented a theoretical model to quantify the stresses causing transient thermal strain in heated concrete. The model was also incorporated into finite element analysis code in ABAQUS for performing the fire safety analysis of concrete structural members.

The literature survey described above shows that there have been numerous research works on the effect of preload on the thermal strain and corresponding stress-strain constitutive relations of OPC concrete, but there is a lack of similar works on other types of concrete. Geopolymer is a novel material that has wide applications in construction industry because its manufacturing involves less CO2 emissions. Geopolymers have excellent thermal stability because of their inorganic feature and framework. Concrete made by geopolymers often has good fire resistance. However, existing research on geopolymer concrete (GPC) related to fire safety is mainly on the thermal and mechanical properties of GPC at or after the high temperature exposure [32,33,34,35], which were obtained from corresponding steady-state tests. For instance, Pan et al. [36] reported an experimental investigation on the stress-strain curves of geopolymer at elevated temperatures. It was found that the hot strength of geopolymer increased with temperature until to 520°C where it reached to the highest strength. Kong and Sanjayan [37] examined the effect of elevated temperature on geopolymer paste, mortar and concrete made using fly ash as a precursor. The parameters examined included the specimen size, the type and size of aggregate, and the type of superplasticizer. Aslani [38] proposed the stress-strain constitutive relationships for normal and high strength GPC exposed to fire, based on the experimental data obtained from the steady-state tests. In contrast, there is very limited work reported on the transient tests of GPC. Only one found in literature is the work done by Junaid et al. [39], which reported the strain histories of fly ash-based GPC when it was subjected to a combined action of heating-loading-heating process. Nevertheless, their existing test results confirmed that the GPC undergoes thermal transient creep, which is much larger than its isothermal creep or shrinkage. To understand the fundamental difference between the OPC concrete and GPC regarding fire resistance, more transient test results are needed since, in real structures, the concrete is usually with mechanical loading already when a fire accident occurs. In this paper we report an experimental study on the mechanical properties of preloaded steel fibre-reinforced GPC when subjected to high temperatures. The transient tests of GPM and GPC specimens with and without steel fibres were carried out by using a modified instron testing machine with additional heating facility. From the temperature-dependent strain results obtained from the transient tests at various preload levels, transient strains are analysed and derived. Some important features are explored and also highlighted.

2 Materials and experiments

2.1 Raw materials and mix design of GPC

Precursors: Ground granulated blast-furnace slag (GGBS), class F fly ash (FA), and salic fume (SF) were used as the combined precursors to form the geopolymer (or alkali activated) binder for producing the geopolymer mortar and/or concrete specimens. The mass ratio of GGBS/FA/SF used in the binder is 3.5/2.0/1.0, which is the same as those used in our previous studies [40,41] where the details about the chemical and physical properties of the GGBS, FA and SF are also provided.

Alkaline activator: Sodium hydroxide (SH) with 95% NaOH with density of 2130 kg/m^3 and sodium silicate (SS) with 30% SiO_2 and 13.5% Na_2O with density of 1510 kg/m^3 were dissolved in the tap water to make alkaline solution for activating the combined binder of GGBS, FA, and SF for producing geopolymer mortar (GPM) and GPC with and without reinforcing steel fibre. The ratio of SH/SS/water used in the alkaline activator is 1/37.5/33.8, which gives the (SS+SH)-to-water ratio of 1.14.

Aggregates: The river sand with sizes up to 3.0 mm and the fineness modulus of 2.70 was used as the fine aggregate. The ratio of sand to binder used in the mortar and concrete mixes was kept being 0.90. The crushed stone was used as the coarse aggregate, the sizes of which are in the range from 5 mm to 10 mm. For GPM the mix consists of binder, alkaline activator, and fine aggregate. For GPC the mix consists of binder, alkaline activator, fine aggregate, and 30% volume fraction of coarse aggregate. Note that the proportions of fine and coarse aggregates used in the present study are smaller than those used in normal concrete mixture. This is because they need to have accommodation to add the steel fibres.

Steel fibre: Straight steel fibre with about 12 mm in length, aspect ratio 45, and 2750 MPa tensile strength was used to produce steel fibre-reinforced GPM and GPC. A single 2% volume fraction of steel fibre was used in both the steel fibre-reinforced GPM and steel fibre-reinforced GPC.

Table 1 shows the mixing details used in the GPM and GPC with and without steel fibre, in which the first letter (S) represents the "steel fibre", the second number (0 or 2) represents the volume fraction of steel fibre, the third and furth letters (CA) represent the "coarse aggregate", and the final number(s) (0 or 30) represent the volume fraction of coarse aggregate. The strength and elastic modulus given in the table are the ambient cylindrical compressive strength and corresponding elastic modulus obtained from our experimental tests.

Table 1 Mixes of GPM and GPC and their mechanical properties

Mix No.	Mixes (units: kg/m^3)									Basic properties	
	GGBS	FA	SF	Fine aggregate	Water	Sodium silicate	NaOH	Steel fibre	Coarse aggregate	Compressive strength (MPa)	Elastic modulus (GPa)
S0CA0	703	201	100	1105	229	254	6.77	\	\	49.9	11.1
S2CA0	689	197	98	1083	224	249	6.63	157	\	84.4	12.3
S0CA30	492	141	70	774	160	178	4.74	\	900	65.8	16.3
S2CA30	483	138	69	758	157	174	4.64	109.9	900	76.6	16.1

2.2 Preparation of specimens

The following processes were employed for mixing the GPM and GPC with and without steel fibre (See Fig. 1).

(1) **Dry mixing**: Coarse aggregate (for GPC), fine aggregate, GGBS, FA, and SF were mixed together using a hand-held mixer for two minutes. After the initial mixing, steel fibre (only for steel fibre-reinforced GPM and GPC) was added into the mixer for additional three minutes of dry mixing.

(2) **Alkaline activator preparation**: Sodium hydroxide was dissolved in water and stirred for five minutes. Sodium silicate was then added into the sodium hydroxide solution and mixed for another five minutes to form the alkaline activator.

(3) **Wet mixing**: The alkaline activator prepared in step 2 was added into the mixer containing the solid constituents formed in step 1. Wet mixing was performed for approximately four minutes to ensure the mixture has been evenly and properly mixed.

(4) **Casting and vibrating**: The freshly mixed GPM or GPC with or without steel fibre was poured into the cylindrical plastic moulds of 50 mm in diameter and 100 mm in length. The moulds were vibrated for one minute to remove air bubbles and to ensure the fresh mixture was properly compacted.

(5) **Initial curing and demoulding**: After casting and vibrating, the specimens in the moulds were stored in the room with temperature about 20°C for 24 hours. After the 24-hour initial curing, the specimens were demoulded from the moulds.

(6) **Standard curing**: The demoulded specimens were then relocated to a curing room with ambient temperature (~20°C) and a relative humidity of over 90% to have a 28-day standard curing.

(7) **Surface polishing**: After the specimens had the 28-day standard curing, the two end surfaces of each cylindrical specimen were polished to ensure the axial compressive load would be uniformly applied to the specimen during the tests.

(a) Concrete mixing (b) Concrete casting (c) Concrete curing (d) Surface polishing

Fig. 1 Preparation of GPM and GPC specimens with and without steel fibre

2.3 Mechanical and thermal loading tests

The combined mechanical and thermal tests (transient tests) were conducted in Wuhan University, China. Fig. 2 shows the schematic and corresponding equipment/devices used in the tests, which include an Instron universal testing machine with maximum loading capacity of 300 kN, a mobile GW900 cylindrical electric furnace with heating temperature up to 1200°C, and a digital image correlation (DIC) camera with a displacement resolution of 0.001 mm. During the test, the cylindrical specimen was first fitted into the place between the two loading rods in the Instron machine. The electric furnace was then mounted around the specimen. During the test the mechanical load was first applied at the loading rate of 0.8 MPa/s until the preset load (preload) was reached. After then the mechanical load was kept unchanged and the electric

furnace with the heating rate of 3ºC/min was switched on. After the target temperature was reached the heating was stopped but the test continued for another two hours to ensure the inside temperature of the specimen also reached to the target temperature.

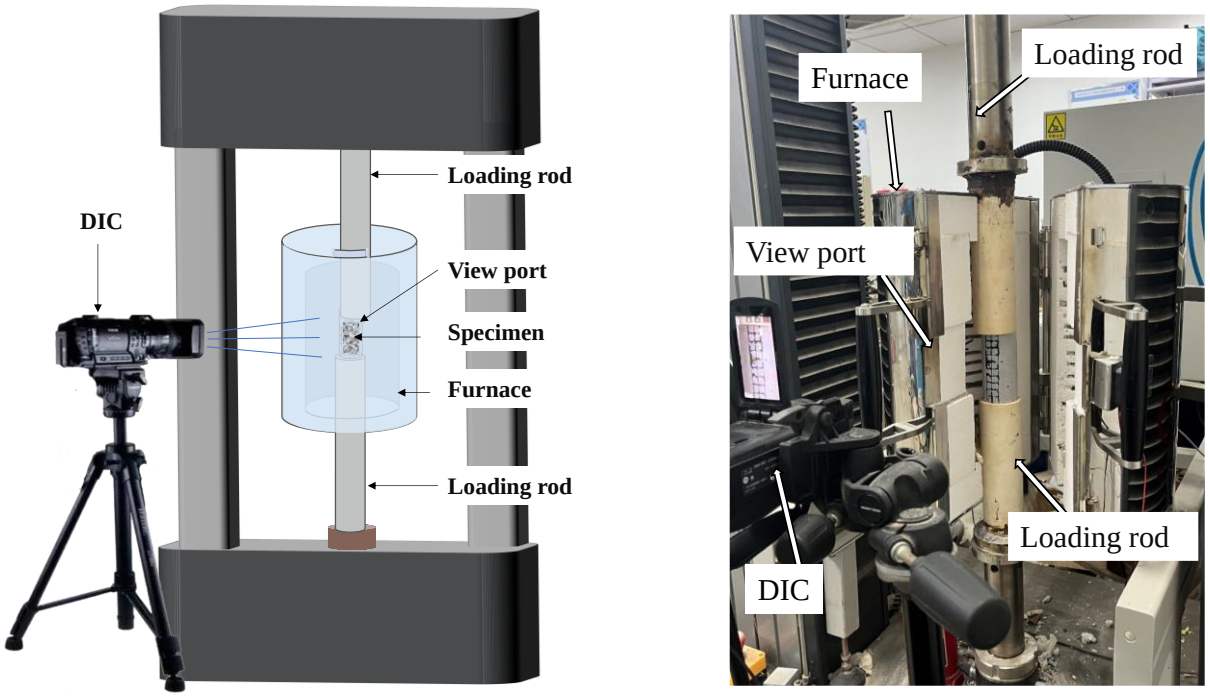

(a) Schematic of test (b) Photo of test equiment

Fig. 2 Experimental equipment

During the test the mechanical loading history was automatically recorded by a computer connected to the Instron machine. The temperature inside the furnace was monitored and controlled by three thermocouples located at different places inside the furnace. The average temperature of the three thermocouples was also recorded by a computer as the temperature history of the furnace. The strain history of the specimen during the mechanical loading and combined mechanical and thermal loadings was recorded via DIC through a rectangular observation hole installed in front of the furnace. The DIC is a new technology for remotely measuring the displacements/strains on the surface of specimens by capturing images during mechanical and thermal testing. The strains/displacements measured by the DIC can be located in the target area which is more accurate than the conventional methods by using strain and/or displacement gauges, particularly for the tests involving both heating and loading. Note that the transient test is very time consuming. The typical time for heating a specimen to 700ºC is about 4 hours, and thus the total time for completing the transient test to temperature 700ºC is about 6-7 hours. Fig. 3 describes the loading path for the mechanical and thermal loadings and corresponding strain evolution during the test.

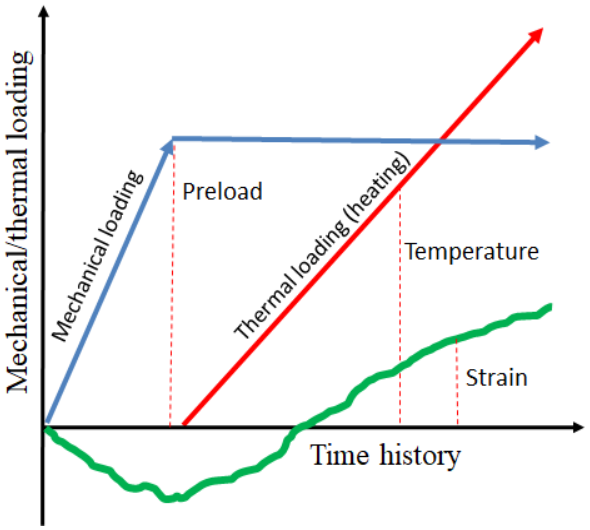

Fig. 3 Mechanical and thermal loadings and strain evolution in specimen

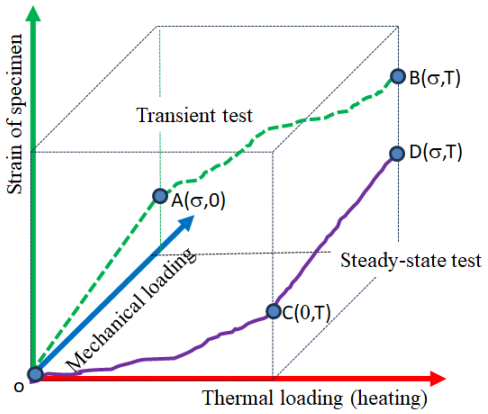

ε_A: strain after mechanical loading σ under ambient temperature
ε_B: strain after mechanical loading σ followed by thermal loading T
ε_C: strain after thermal loading T under no mechanical loading
ε_D: strain after thermal loading T followed by mechanical loading σ

Fig. 4 Description of strain evolution in concrete specimen under different loading paths

3 Results and discussion

3.1 Definition of free thermal expansion, initial mechanical, instantaneous mechanical, and transient strains

Consider the axial strain of the cylindrical specimen when it is subjected to combined mechanical and thermal loadings. We consider two different loading paths as shown in Fig. 4. One is called the steady-state test (path oCD), in which the specimen is heated first from a room temperature to a target temperature T, where the axial strain evolution of the specimen is represented by the path o→C and the corresponding strain at point C is known as the thermal strain of free expansion $\varepsilon_C=\varepsilon_{th}(0,T)$ (TSoFE). After the target temperature T has been reached, the temperature remains unchanged while the mechanical load is applied from 0 to a target stress σ, where the axial strain evolution of the hot specimen is represented by the path C→D and the corresponding strain at point D is $\varepsilon_D=\varepsilon_{th}(0,T)+\varepsilon_{me}(\sigma,T)$, where $\varepsilon_{me}(\sigma,T)$ is instantaneous mechanical strain generated by applied stress under a constant temperature T. The other is called the transient test (path oAB), in which the specimen is mechanically loaded first from 0 to a target stress σ, where the axial strain evolution of the specimen is represented by the path o→A and the corresponding strain at point A is known as initial mechanical strain $\varepsilon_A=\varepsilon_{me}(\sigma,0)$. After the target stress σ has been reached, the axial stress in the specimen remains unchanged while the thermal heating is applied from room temperature to a target temperature T, where the axial strain evolution of the stressed specimen is represented by the path A→B and the corresponding strain at point B is $\varepsilon_B=\varepsilon_{me}(\sigma,0)+\varepsilon_{AB}(\sigma,T)$, where ε_{AB} is the thermal strain of stressed expansion of the specimen under the constant stress σ. Note that although the final temperature and final stress in the specimen designed in the two loading paths are exactly the same, the final strains in the specimen generated by the two loading paths are different, that is $\varepsilon_B\neq\varepsilon_D$, as indicated in Fig. 4. In literature the strain difference between points B and D obtained from corresponding transient and steady-state tests is referred to as the transient and creep strains [1,3,5,9], that is,

$$\varepsilon_{tr}(\sigma,T)+\varepsilon_{cr}(\sigma,T)=\varepsilon_B(\sigma,T)-\varepsilon_D(\sigma,T)=\varepsilon_B(\sigma,T)-\varepsilon_{th}(0,T)-\varepsilon_{me}(\sigma,T) \quad (1)$$

where $\varepsilon_{tr}(\sigma,T)$ and $\varepsilon_{cr}(\sigma,T)$ are the transient and creep strains, respectively. Since the period of heating in the transient test is normally very short (several hours), the creep strain would be expected to be very small

and thus could be ignored. Under this assumption, the transient strain ε_{tr} can be determined experimentally in terms of the TSoFE, ε_{th}, the instantaneous mechanical strain, ε_{me}, obtained from the steady-state test, and the total strain, ε_B, obtained from the transient test, as follows,

$$\varepsilon_{tr}(\sigma,T) = \varepsilon_B(\sigma,T) - \varepsilon_{th}(0,T) - \varepsilon_{me}(\sigma,T) \quad (2)$$

Note that the transient strain reflects the influence of the preload on the thermal strain, and it is only exhibited on the first heating cycle, but not the first cooling cycle. Also, any subsequent heating and cooling cycles do not exhibit transient strain [1]. Eq.(2) also shows the difference between the thermal strain of free expansion and the transient strain. This means that the thermal expansion coefficient obtained from free expansion tests cannot be directly used for calculating the transient strain. In addition, concrete is a composite material involving binder and aggregate which have different thermal and mechanical properties. Therefore, the transient strain depends on not only the temperature and prestress level but also the materials and their proportions used to mix the concrete.

3.2 Strain results obtained from transient tests

Fig. 5 shows the total strains of the specimens recorded during our transient tests when the temperature rises from 20°C to 700°C. The specimens tested included the GPM (S0CA0 and S2CA0) and GPC (S0CA30 and S2CA30) with and without steel fibre. For each type of the mixes the transient tests were carried out by using four different preload levels defined by the stress ratio $n=\sigma/f_{co}$, including one with $n=0$ representing the free expansion, where σ is the prestress applied to the specimen before it was heated and f_{co} is the compressive strength of the specimen at ambient temperature. Note that, since the specimens (S0CA0, S2CA0, S0CA30, and S2CA30) have different ambient compressive strengths (see Table 1), their prestresses actually applied to them are different because they have the same preload level. For example, S2CA0 has the highest f_{co}, thus the actual prestress σ applied to it is the largest because its n value has to be the same to other three specimens. It can be seen from Fig. 5a that, for GPM without steel fibre (S0CA0) the TSoFE increases almost linearly with temperature until about 200°C. When the temperature rises from 200°C to 500°C the TSoFE does not have remarkable increase, indicating that the shrinkage of geopolymer started before the temperature 200°C and after the temperature 200°C the shrinkage of geopolymer was almost balanced by the thermal expansion of sand. After the temperature exceeds 500°C, the TSoFE increases slightly with increased temperature, which was mainly due to the enlargement of thermal cracking. The results of TSoFE (n=0) shown in Fig. 5 can be used to calculate the thermal expansion coefficient. However, as the TSoFE in each specimen is not linearly related to the temperature, the thermal expansion coefficient is not a constant but the temperature dependent. The detailed discussion about the temperature dependent behaviours of thermal expansion coefficient of GPM and GPC can be found in Ref. [40].

For preloaded specimens, when the temperature rises from 20°C to 200°C, their total strain in each specimen also increases almost linearly with temperature, but the rate of increase is different between the specimens with different preload levels. The specimen with higher preload level has lower increase rate. This is mainly attributed to the influence of the mechanical strain, as the mechanical strain also increases with increased temperature because the modulus of elasticity decreases with increased temperature. When the temperature rises from 200°C to 600°C, the total strain in each specimen was found to decrease remarkably with increased temperature. The specimen with higher preload level has quicker reduction in the strain. This implies that, apart from the mechanical strain, the transient strain plays an important role in the strain reduction in this temperature region. After the temperature exceeds 600°C, the stiffness of the specimens

becomes very weak regardless of its preload level and thus a small increase in temperature leads to a large increase in compressive strain, indicating that under the action of preload the specimen almost reaches to its failure state.

Fig. 5b shows the variation of the total strain with temperature in GPC specimens without steel fibre (S0CA30), recorded during their transient tests. Like those shown in Fig. 5a, the strains shown in Fig. 5b can be also characterised in terms of three temperature zones. One is from temperature 20°C to 200°C, where the strain is mainly contributed by the thermal and mechanical strains. The former is linearly proportional to temperature and the latter is influenced not only by the preload level but also by the temperature. One is from the temperature 200°C to 600°C, where the TSoFE increases with temperature but the rate of increase reduces because of the shrinkage of geopolymer. The preload-induced compressive strain increases quickly with increased temperature, indicating the fast development of the transient strain in that zone. One is after the temperature exceeds 600°C, where the specimens are thermally unstable and thus the small increase in temperature leads to a substantial increase in compressive strain. Overall, for the same temperature and identical preload level the GPC specimens have slightly higher TSoFE but much lower compressive strains than GPM specmens, indicating that coarse aggregate does have effect on the thermal, mechanical, and transient strains of concrete. Note that during the transient test the GPC specimen with n=0.6 was failed at temperature about T=375°C, which was probably due to the localised defect in the specimen caused by the interfacial transition zone surrounding the coarse aggregate.

Figs. 5c and 5d show the variation of the total strain with temperature in the steel fibre-reinforced GPM and GPC specimens, respectively. The overall variation feature of the strains with temperature in the steel fibre-reinforced GPM or GPC specimens is found to be similar to that in the GPM or GPC specimens without steel fibre, indicating that the steel fibre has no remarkable influence on the thermal, mechanical and transient strains of the GPM and GPC. It is noticed that for the same preload level the compressive strain in steel fibre-reinforced GPM (S2CA0) shown in Fig. 5c is generally larger than that in GPM without steel fibre (S0CA0) shown in Fig. 5a. The reason for this is because the steel fibre-reinforced GPM has much higher ambient compressive strength than the GPM. Thus, for the same n value the actual prestress σ applied to the steel fibre-reinforced GPM specimen was much higher than that applied to the GPM without steel fibre, which led the former to have larger compressive strain than the latter.

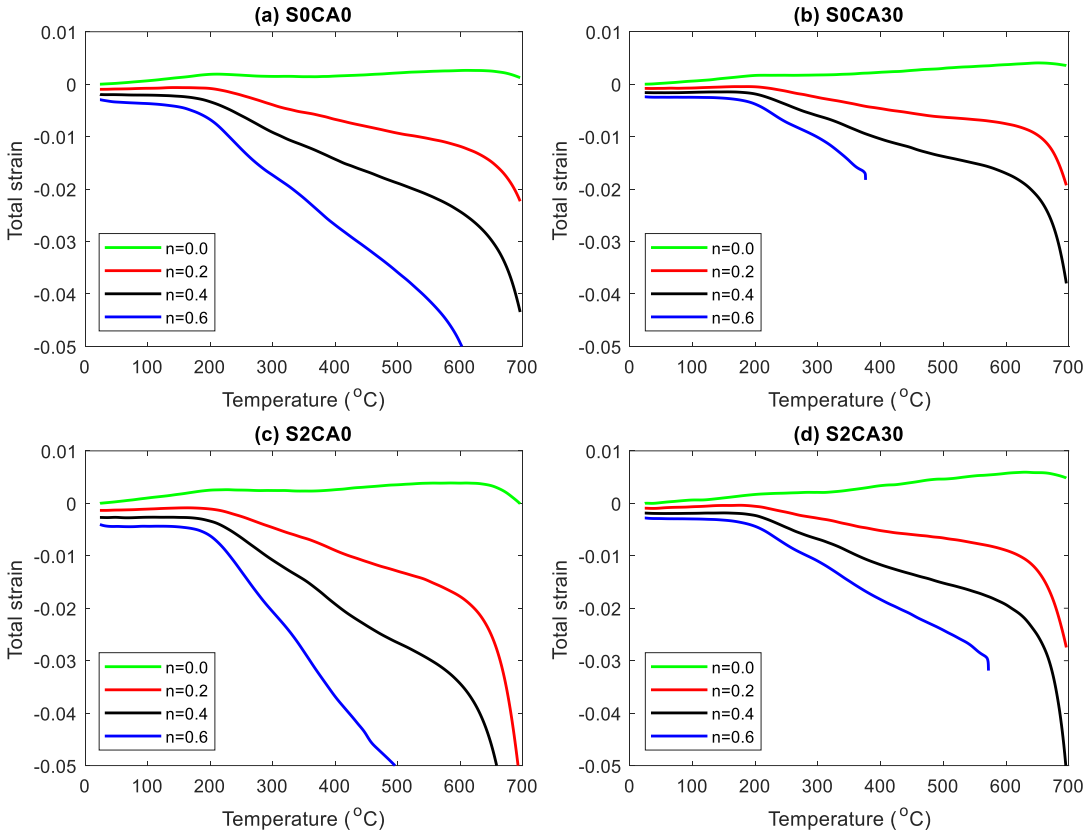

Fig. 5 Total strain of GPM and GPC specimens at various preload levels as a function of temperature

3.3 Transient strains of GPM and GPC with and without steel fibre

According to Eq.(2), for a given preload level the temperature-dependent transient strain can be calculated by using the TSoFE and total strain recorded in the transient tests as shown in Fig. 5, and the instantaneous mechanical strain obtained from the steady-state tests. Fig. 6 shows the normalised stress-strain curves of the GPM and GPC with and without steel fibre, obtained from our steady-state tests at the temperatures of 20, 100, 300, 500, and 700ºC, from which the instantaneous mechanical strains at various preload levels can be obtained directly. The disadvantage of this method is the stress-strain curves that are available only at several temperatures. Alternatively, the instantaneous mechanical strains can be approximately calculated by using the temperature-dependent modulus of elasticity. However, this method gives only the linear part of the strain. Fig. 7 Shows the instantaneous mechanical strains obtained by using these two methods. It can be seen from the figure that the two methods give no significant difference when *n* value is small, or the temperature is not very high. The difference becomes remarkable only when the *n* value and temperature both are high. This is because the strain calculated using the elastic modulus neglects the nonlinear part of the strain, which may be important in the stress-strain curve at high temperature, particularly when the stress is close to the peak stress point.

Based on the thermal, mechanical and total strains, the transient strain is calculated using Eq.(2), the results of which are shown in Fig. 8. It is observed that for temperature below 200ºC the transient strains in all the four mixes are very small and almost negligible, which is different from that of OPC concrete [1,5,9]. For temperature greater than 200ºC the transient strain amplifies with temperature till it is close to the failure temperature where it has an abrupt increase. The larger the preload level, the larger the transient strain.

Overall, for the same preload level and same temperature the GPM has larger transient strain than the GPC no matter whether they have steel fibre, indicating that the binder is the main contributor of the transient strain.

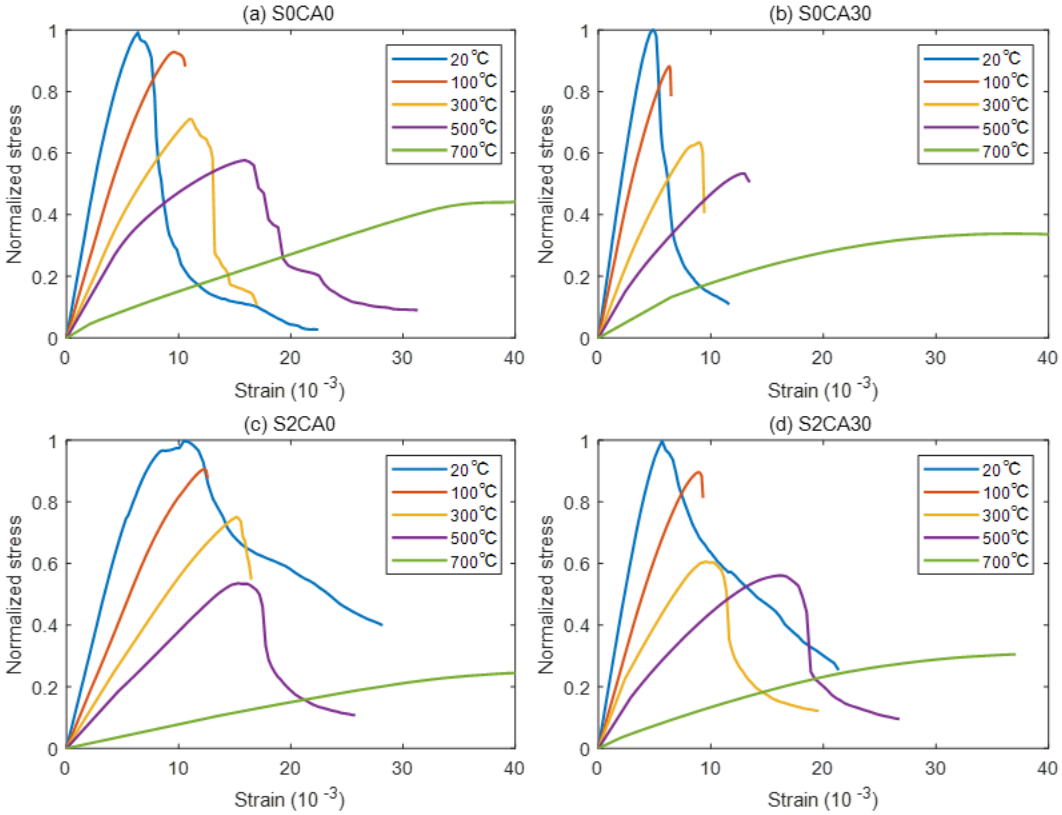

Fig. 6 Normalised stress-strain curves of GPM and GPC with and without steel fibre at various elevated temperatures (ambient compressive strengths of S0CA0, S0CA30, S2CA0 and S2CA30 are f_{co}=49.9, 65.8, 84.4 and 76.6 MPa, respectively).

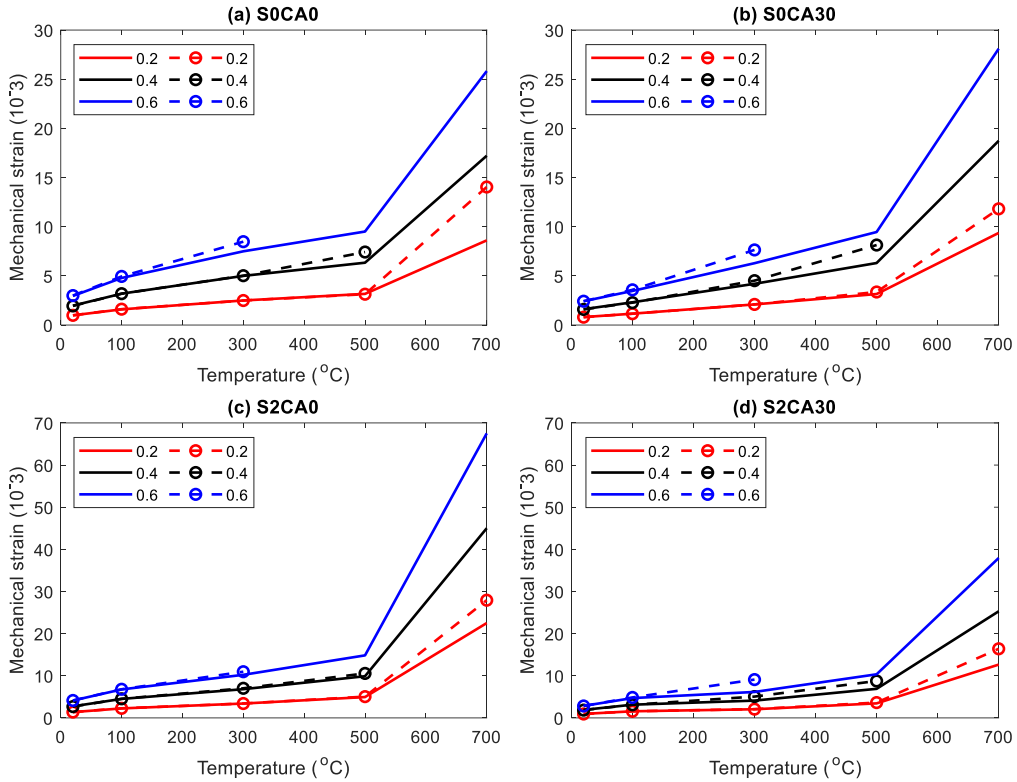

Fig. 7 Instantaneous mechanical strains calculated using two methods (results marked with points are taken directly from stress-strain curve, and results marked with straight line are calculated using elastic modulus, respectively)

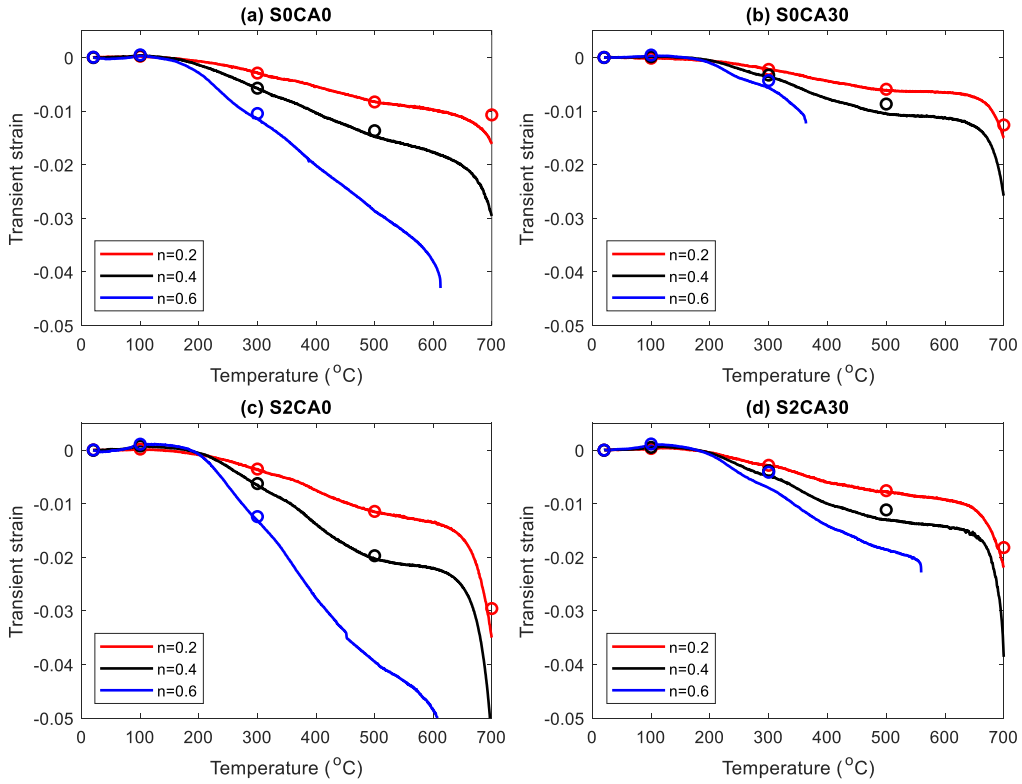

Fig. 8 Transient strain in GPM and GPC with and without steel fibre (results marked with points and lines correspond to the mechanical strains taken directly from stress-strain curve and calculated using elastic modulus)

Figs. 9 and 10 show the detailed comparison of the transient strains between GPM and GPC with and without steel fibre at three different preload levels. It is found that the effect of coarse aggregate on transient strain increases with increased preload level or increased temperature. This kind of effects is further broadened by the addition of the reinforced steel fibre. Note that because the geopolymer and coarse aggregate have different thermal expansion strains the GPC generally has higher localised internal thermal stress than the GPM, which could speed up the failure of the preloaded GPC when the temperature becomes high, even though the ambient compressive strength of GPC is higher than that of GPM. This is why in the transient tests of n=0.6 the GPC specimen with and without steel fibre were failed at temperature 580°C and 375°C, respectively; whereas the corresponding GPM specimens did not.

Figs. 11 and 12 show the detailed comparisons of transient strains between steel fibre-reinforced and non-reinforced GPM and GPC at three different preload levels. It is observed that the steel fibre has little effect on the transient strain of GPC, but remarkable effect on the transient strain of GPM. The latter is due to the higher ambient compressive strength of the GPM with steel fibre, which leads to higher prestress applied to the specimen because of the same n value used. If the actual prestress applied to the GPM specimens with and without steel fibre (not the ratio) were the same, the transient strains of these two specimens would not be so different.

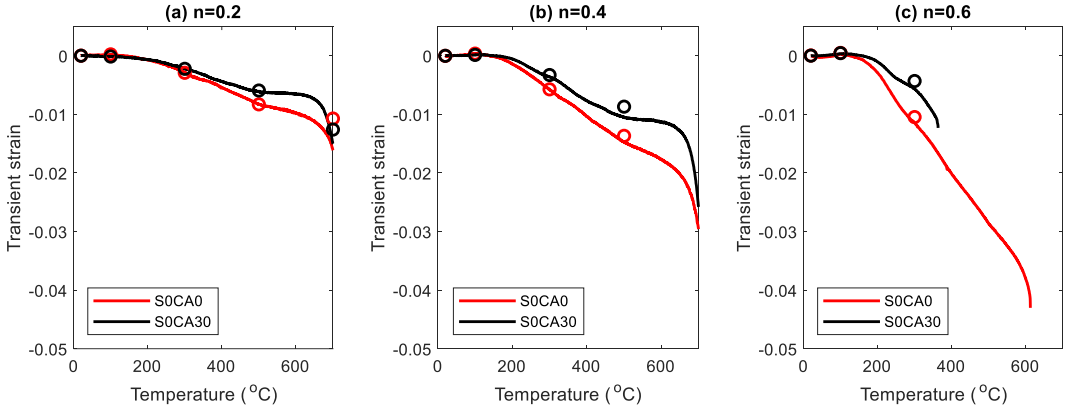

Fig. 9 Effect of coarse aggregate on transient strain in specimens without steel fibre (results marked with points and lines correspond to the mechanical strains taken directly from stress-strain curve and calculated using elastic modulus)

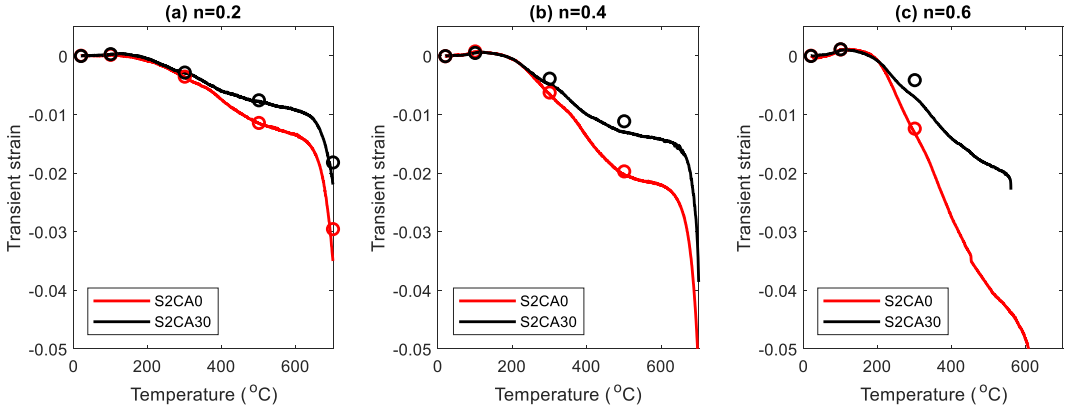

Fig. 10 Effect of coarse aggregate on transient strain in specimens with steel fibre (results marked with points and lines correspond to the mechanical strains taken directly from stress-strain curve and calculated using elastic modulus)

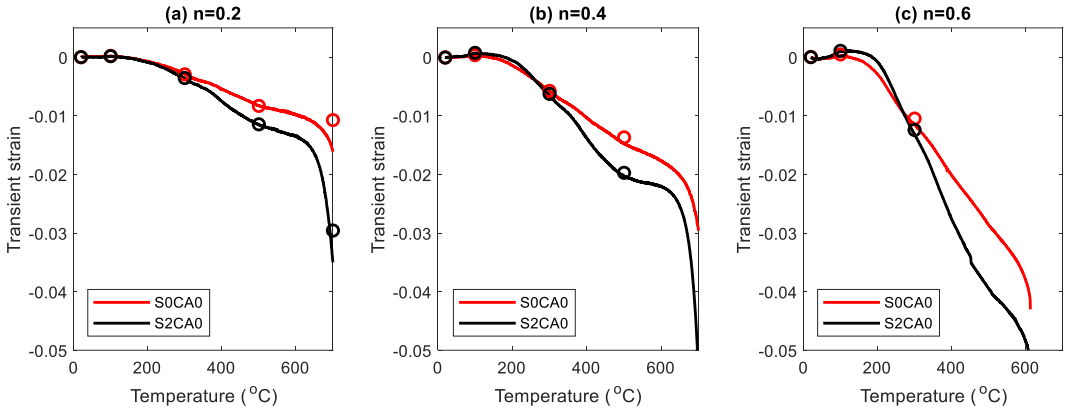

Fig. 11 Effect of steel fibre on transient strain of GPM specimens (results marked with points and lines correspond to the mechanical strains taken directly from stress-strain curve and calculated using elastic modulus)

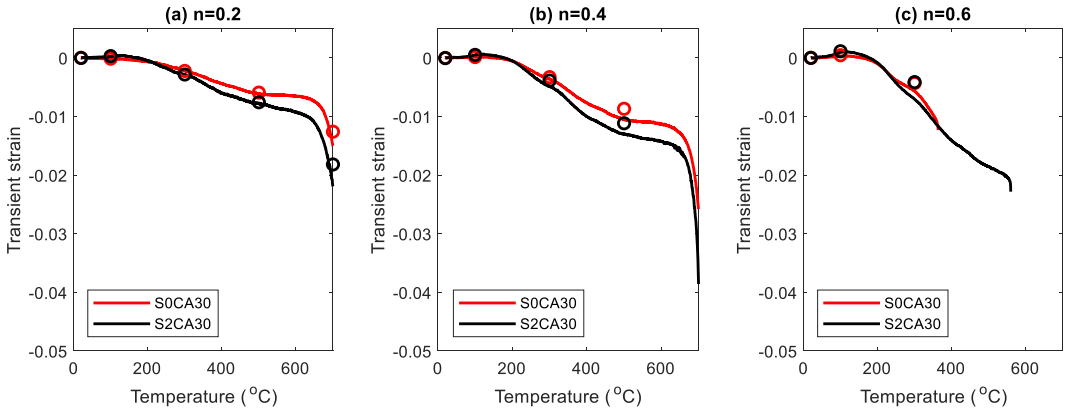

Fig. 12 Effect of steel fibre on transient strain of GPC specimens (results marked with points and lines correspond to the mechanical strains taken directly from stress-strain curve and calculated using elastic modulus)

4 Approximate models of transient strain

The transient strains shown in Fig. 8 are obviously different at different preload levels and different temperatures, as well as in different mixes, indicating the influences of the preload, temperature, and constituents of the mix. However, a common feature of them is that when the temperature is below a threshold temperature, the transient strain is very small and can be neglected. When the temperature is close to the failure temperature, the transient strain has a sharp increase, which could be due to the large plastic strain and/or the thermal instability of the material [42]. These two features are significantly different from that of OPC concrete [1,5,9]. According to the transient strains shown in Fig. 8, the following empirical formulas are proposed for the GPM and GPC with and without steel fibre.

For temperature below threshold temperature (T_{thr}):

$$\varepsilon_{tr}(\sigma, T) = 0 \tag{3}$$

For temperature above threshold temperature (T_{thr}) but below failure temperature (T_{fail}):

$$\varepsilon_{tr}(\sigma, T) = k\left(\frac{\sigma}{f_{co}}\right)^{m}\left(\frac{T}{T_{thr}} - 1\right) \tag{4}$$

where k and m are the fitting constants to be determined based on the experimentally obtained data, T_{thr} and

T_{fail} are the threshold and failure temperatures, respectively. The values of k, m, T_{thr}, and T_{fail} for the present four mixes are given in Table 2. Eq.(4) can be easily incorporated into the concrete constitutive equation for conducting fire performance analysis of concrete structures in fire [9,44].

Fig. 13 shows the comparisons of transient strains obtained from proposed empirical formula and experimental results. It is observed from Fig.13 that the use of the linear relationship between the transient strain and temperature appears acceptable for all of the four mixes. This seems to be consistent with the results of OPC concrete reported in literature [5,42]. Also, it is observed from the figure that, the rate of increase of the transient strain with preload is smaller in the GPC specimens than in the GPM specimens, and the increase in transient strain seems not linearly proportional to the increase in preload, which thus requires a power function to represent it; whereas for OPC concrete the relationship between the transient strain and preload level is almost linear [5]. Finally, the slight differences in both the threshold and failure temperatures between the four mixes reflect the distinct influence of sand, aggregate and steel fibre on the evolution of transient strain during the heating process.

The present transient strain formulas can be incorporated into the stress-strain constitutive equations of GPM and GPC to perform the stress analysis of GPC structures which are already loaded when exposed to elevated temperatures. For example, when we use commercial finite element analysis software, we need to define the stress-strain relationship of the material in which the strain is the stress-induced mechanical strain at a constant temperature. The total strain of the material is the sum of the thermal and mechanical strains if the transient strain is not considered. When the transient strain is considered, the total strain is the sum of the thermal, mechanical, and transient strains. To perform the finite element analysis using commercial software, we have to add the transient strain either into the thermal strain by modifying the thermal expansion coefficient or into the mechanical strain by modifying the stress-strain relationship. Since the transient strain is not only dependent on the temperature but also on the stress, it would be more convenient to add the transient strain into the mechanical strain by modifying the stress-strain equation as described in Ref. [1,9] for OPC concrete.

Table 2 Parametric values used in empirical formulas of transient strain

Parameter	S0CA0	S0CA30	S2CA0	S2CA30
m	1.3	0.85	1.3	0.85
k	2.49×10^{-2}	1.01×10^{-2}	4.17×10^{-2}	0.61×10^{-2}
T_{thr} (°C)	160	160	180	180
T_{fail} (°C)	653 (n=0.2) 640 (n=0.4) 595 (n=0.6)	640 (n=0.2) 627 (n=0.4) 360 (n=0.6)	623 (n=0.2) 605 (n=0.4) 576 (n=0.6)	635 (n=0.2) 617 (n=0.4) 553 (n=0.6)

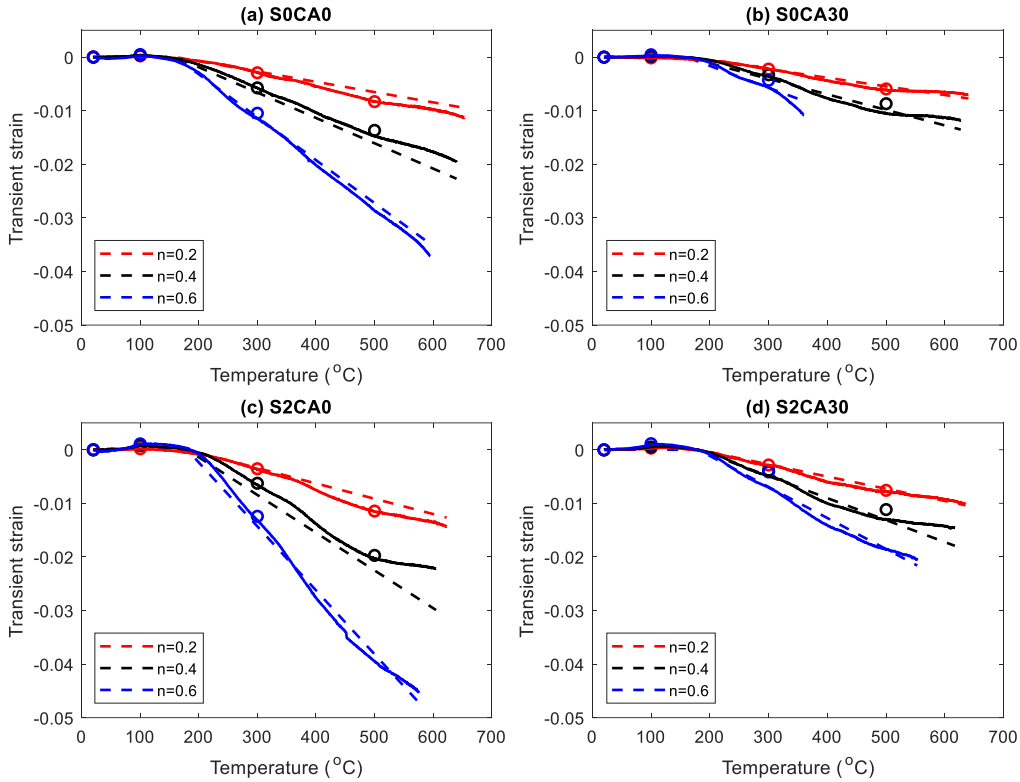

Fig. 13 The comparison between proposed empirical formula and experimental data (points and straight lines are experimental results, and dash-lines are calculated using empirical formula)

5 Conclusions

In this paper we have presented an experimental study on the axial deformation of GGBS-FA-SF blended GPM and GPC with and without steel fibre when they are subjected to both mechanical and thermal loadings. The transient tests of the concrete were conducted in Instron testing machine with heating facility. The transient axial deformation of the tested specimens was recorded using digital image correlation camera. By using the experimentally obtained temperature-dependent thermal strains of the specimen with different preloads the transient strains of the GPM and GPC with and without steel fibre have been analysed and evaluated. From the results obtained we have the following conclusions.

1) The transient strain of GPM or GPC is very small and could be neglected if the temperature is below its threshold temperature, which is around 200ºC. This feature seems considerably distinctive to that of the ordinary Portland cement concrete.
2) The transient strain of GPM is much higher than that of GPC regardless of whether they have steel fibre or not, indicating that the coarse aggregate can effectively compensate the development of transient strain.
3) The steel fibre has insignificant influence on the transient strain of GPM and GPC because of its small volume fraction used in the mixes. However, the steel fibre may affect the threshold and failure temperatures of the GPM and GPC.
4) The transient strain could be modelled as a linear function of temperature although the proportional constants may be different for GPM and GPC with and without steel fibre. This kind of temperature-dependent feature is similar to that of the OPC concrete.
5) The relationship between the transient strain and preload could be modelled by using a power function.

The power coefficient used for the GPM is different from that used for the GPC. This kind of preload-dependent feature seems different from that of the OPC concrete.

Acknowledgements - The authors would like to acknowledge the financial support received from the National Natural Science Foundation of China under grants (No. 52078300 and No. 51978406), the Marie Skłodowska-Curie Individual Fellowships (H2020-MSCA-IF-2020) under grant No. 101022142 (TemGPC), and the Royal Society Joint Project with NSFC, China under grant No. IEC\NSFC\201077.

References

[1] J.A. Purkiss, L.Y. Li, Fire Safety Engineering, Design of Structures (3rd edition). CRC Press, Oxford (2013).

[2] G.A. Khoury, B.N. Grainger, P.J.E. Sullivan, Transient thermal strain of concrete; literature review, conditions within specimen and behaviour of individual constituents, Magazine of Concrete Research 37(132) (1985) 131-144.

[3] G. Torelli, P. Mandal, M. Gillie, V.X. Tran, Concrete strains under transient thermal conditions: A state-of-the-art review, Engineering Structures 127 (2016) 172-188.

[4] C.T. Hansen, L. Eriksson, Temperature change effect on behaviour of cement paste, mortar, and concrete under load, Journal Proceedings 63(4) (1966) 489-504.

[5] Y. Anderberg, S. Thelandersson, Stress and deformation characteristics of concrete at high temperatures 2. Experimental investigation and material behaviour model, Lund Institute of Technology, 1976.

[6] G. A. Khoury, Strain of heated concrete during two thermal cycles. Part 1: strain over two cycles, during first heating and at subsequent constant temperature, Magazine of Concrete Research 58(6) (2006) 367–385

[7] G. A. Khoury, Strain of heated concrete during two thermal cycles. Part 2: strain during first cooling and subsequent thermal cycle, Magazine of Concrete Research 58(6) (2006) 387–400.

[8] G. A. Khoury, Strain of heated concrete during two thermal cycles. Part 3: isolation of strain components and strain model development, Magazine of Concrete Research 58(7) (2006) 421–435.

[9] L.Y. Li, J.A. Purkiss, Stress-strain constitutive equations of concrete material at elevated temperatures, Fire Safety Journal 40(7) (2005) 669-686.

[10] M.A. Youssef, M. Moftah, General stress-strain relationship for concrete at elevated temperatures, Engineering Structures, 29 (10) (2007) 2618-2634.

[11] A. Sadaoui, A. Khennane, Effect of transient creep on the behaviour of reinforced concrete columns in fire, Engineering Structures 31(9) (2009) 2203-2208.

[12] U. Schneider, M. Schneider, An advanced transient concrete model for the determination of restraint in concrete structures subjected to fire, Journal of Advanced Concrete Technology 7(3) (2009) 403-413.

[13] U. Schneider, M. Schneider, Experimental study of the advanced transient concrete model on reinforced concrete columns during fire exposure, Open Construction and Building Technology Journal 4 (2010) 79-87.

[14] K. Toyoda, H. Yamashita, M. Tokoyoda, T. Hirashima, H. Uesugi, Experimental study on transient strain of 100N/mm2 high strength concrete exposed to fire, Journal of Structural and Construction Engineering 75(648) (2010) 453-460.

[15] A.M. Knaack, Y.C. Kurama, D.J. Kirkner, Compressive stress-strain relationships for North American concrete under elevated temperatures, ACI Materials Journal 108(3) (2011) 270-280.

[16] T. Gernay, J.M. Franssen, A formulation of the Eurocode 2 concrete model at elevated temperature that includes an explicit term for transient creep, Fire Safety Journal 51 (2012) 1-9.
[17] S.S. Huang, I.W. Burgess, Effect of transient strain on strength of concrete and CFT columns in fire - Part 1: Elevated-temperature analysis on a Shanley-like column model, Engineering Structures 44 (2012) 379-388.
[18] J. Tao, X. Liu, Y. Yuan, L. Taerwe, Transient strain of self-compacting concrete loaded in compression heated to 700 °c, Materials and Structures 46(1-2) (2013) 191-201.
[19] F. Aslani, Prestressed concrete thermal behaviour, Magazine of Concrete Research 65(3) (2013) 158-171.
[20] T.T. Nguyen, K.H. Tan, Thermal-induced restraint forces in reinforced concrete columns subjected to eccentric loads, Fire Safety Journal 69 (2014) 136-146.
[21] J. Ožbolt, J. Bošnjak, G. Periškić, A. Sharma, 3D Numerical analysis of reinforced concrete beams exposed to elevated temperature, Engineering Structures 58 (2014) 166.
[22] L. Lu, Y. Yuan, R. Caspeele, L. Taerwe, Influencing factors for fire performance of simply supported RC beams with implicit and explicit transient creep strain material models, Fire Safety Journal 73 (2015) 29-36.
[23] J.Y. Hwang, H.G. Kwak, J. Hwang, Y. Lee, W.J. Kim, Fire-resistant capacity of RC structures considering time-dependent creep strain at elevated temperature, Magazine of Concrete Research 68(15) (2016) 782-797.
[24] Y.W. Lee, G.Y. Kim, N. Gucunski, G.C. Choe, M.H. Yoon, Thermal strain behavior and strength degradation of ultra-high-strength-concrete, Materials and Structures 49(8) (2016) 3411-3421.
[25] M. Yoon, G. Kim, Y. Kim, T. Lee, G. Choe, E. Hwang, J. Nam, Creep behavior of high-strength concrete subjected to elevated temperatures, Materials 10(7) (2017) 781.
[26] Y. Yao, K. Wang, X. Hu, Thermodynamic-based elastoplasticity multiaxial constitutive model for concrete at elevated temperatures, Journal of Engineering Mechanics 143(7) (2017) 04017039.
[27] K.A. Mahmoud, Interaction diagrams and failure criteria for RC columns subjected to high temperature, Journal of Structural Fire Engineering 11(3) (2020) 347-378.
[28] H. Al-Thairy, A simplified method for steady state and transient state thermal analysis of hybrid steel and FRP RC beams at fire, Case Studies in Construction Materials 13 (2020) e00465.
[29] A. Zawadowska, L. Giuliani, K.D. Hertz, Experimental study on the mechanical properties of fire exposed concrete, Safety Science 142 (2021) 105357.
[30] K. Fan, J. Li, Z. He, Q. Liu, Y. Yao, Transient creep strain of fly ash concrete at elevated temperatures, Magazine of Concrete Research 74(22) (2022) 1176 - 1187.
[31] A.M. Abubaker, C.T. Davie, A generalised model for direct prediction of stresses in concrete at high temperatures, Magazine of Concrete Research 75(4) (2023) 176-186.
[32] M. Lahoti, K.H. Tan, E.H. Yang, A critical review of geopolymer properties for structural fire-resistance applications, Construction and Building Materials 221 (2019) 514-526.
[33] M. Amran, S.S. Huang, S. Debbarma, R.S.M. Rashid, Fire resistance of geopolymer concrete: A critical review, Construction and Building Materials 324 (2022) 126722.
[34] Q.F. Song, M.Z. Guo, T.C. Ling, A review of elevated-temperature properties of alternative binders: Supplementary cementitious materials and alkali-activated materials, Construction and Building Materials, 341 (2022) 127894.
[35] W.L. Tu, M.Z. Zhang, Behaviour of alkali-activated concrete at elevated temperatures: A critical review, Cement and Concrete Composites 138 (2023) 104961.

[36] Z. Pan, J.G. Sanjayan, Stress–strain behaviour and abrupt loss of stiffness of geopolymer at elevated temperatures, Cement and Concrete Composites 32(9) (2010) 657-664.
[37] D.L.Y. Kong, J.G. Sanjayan, Effect of elevated temperatures on geopolymer paste, mortar and concrete, Cement and Concrete Research 40(2) (2010) 334-339.
[38] F. Aslani, Thermal performance modelling of geopolymer concrete, Journal of Materials in Civil Engineering 28(1) (2016) 04015062.
[39] M.T. Junaid, A. Khennane, O. Kayali, A. Sadaoui, D. Picard, M. Fafard, Aspects of the deformational behaviour of alkali activated fly ash concrete at elevated temperatures, Cement and Concrete Research 60 (2014) 24-29.
[40] M. Yu, H. Lin, T. Wang, F. Shi, D. Li, Y. Chi, L.Y. Li, Experimental and numerical investigation on thermal properties of alkali-activated concrete at elevated temperatures, Journal of Building Engineering 74 (2023) 106924.
[41] M. Yu, T. Wang, Y. Chi, D. Li, L.Y. Li, F. Shi, Residual mechanical properties of GGBS-FA-SF blended geopolymer concrete after exposed to elevated temperatures, Construction and Building Materials 411 (2024) 134378.
[42] K. Fan, D. Li, L.Y. Li, J. Wu, Effect of temperature gradient on transient thermal creep of heated and stressed concrete in transient state tests, Construction and Building Materials 222 (2019) 839-851.
[43] G. Torelli, M. Gillie, P. Mandal, V.X. Tran, A multiaxial load-induced thermal strain constitutive model for concrete, International Journal of Solids and Structures 108 (2017) 115-125.
[44] A.M. Abubaker, C.T. Davie, A generalised model for direct prediction of stresses in concrete at high temperatures, Magazine of Concrete Research 75(4) (2023) 176-186.